Simulating creaming behavior in an emulsion using the lattice Boltzmann method

Mauro van der Werf
Student number: 4910141

TU Delft,
Faculty of Applied Sciences,
BSc program Applied Physics

Delft, January 2023

Supervisor:
Dr. Bijoy Bera
Examination Committee:
Prof. Dr. Chris Kleijn
Dr. Orest Shardt

Contents

Abstract

Oil-in-water emulsions are very common in industrial processes, and understanding the factors governing emulsification and de-emulsification is crucial. A mechanism through which de-emulsification commonly takes place is coalescence, being the act of two dispersed-phase droplets coming together to create a single larger droplet. Due to density differences, it is common for dispersed phase droplets to form a creaming layer at the top of the emulsion, increasing the likelihood of coalescence and therefore de-emulsification. The goal of this thesis is to use the lattice Boltzmann method to simulate the rising of a dispersed phase oil droplet towards a creaming layer due to buoyancy effects and to quantify the effect of the viscosities of both phases on the velocity with which aforementioned droplet rises. This is done using the Shan-Chen psuedopotential method.

After introducing gravity into the simulation the the droplet is allowed to reach a terminal velocity v_t. This is done for independently varying viscosities for both the dispersed phase and continuous phase (ν_d and ν_c respectively). A weakly inverse relation was found between v_t and ν_c. An estimation for the terminal velocity of a droplet rising due to creaming behavior is found by cancelling drag force found from Stokes' law against the buoyancy force [1]. Found results were not in agreement with said estimation. Different explanations for this discrepancy are varying droplet diameters, varying droplet densities, droplet deformation and high velocity fluctuations. The terminal velocities were also compared to the ratio between the viscosity of both phases, but no correlation was found.

1 | Introduction

Coalescence is defined as the event of two or more elements coming together to create a single larger entity. In the context of emulsions, being defined as the mixture of two or more immiscible fluids, the coalescence of two droplets of the same phase gives rise to a larger degree of separation between the two phases that the emulsion consists of. Two-phase systems such as oil-in-water emulsions are very common in industrial processes. Therefore knowledge of the mechanisms that influence such phases is crucial. To illustrate this point, we will compare the seemingly very different techniques of processing crude oil and making mayonnaise. For the former, the goal is to separate oil from the water that is present inside crude oil [2]. To achieve this, the droplets in the oil-phase are made to coalesce as much as possible, as to create a single entity of oil and a single entity of water that can be separated from each other. In the case of mayonnaise however, the goal is mix the two phases as evenly as possible, as to make an even mixture of oil and water to serve as a basis for the mayonnaise, as opposed to water filled with concentrated clumps of oil [3]. As illustrated by these two examples, both emulsification and demulsification, and therefore the degree in which coalescence takes place, is crucial in many processes that span a wide range of industries and use-cases.

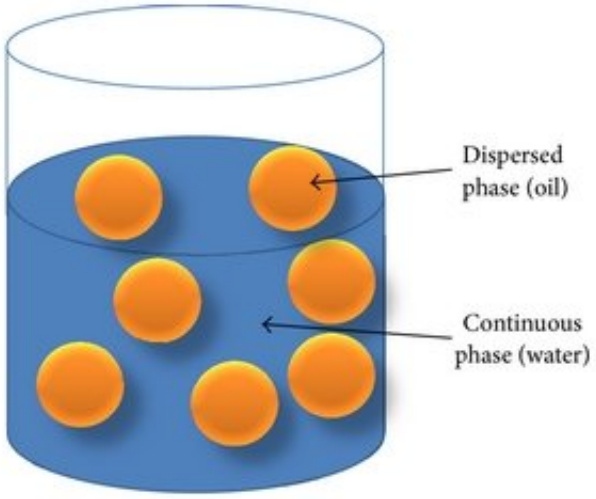

Figure 1.0.1: A schematic view of an oil-in-water emulsion [4].

Research has been done on the subject of emulsification, in particularly in the context of food processing. The mechanisms of demulsification however, have seen somewhat less research [5]. As early as 1978, D.T. Wasan et al. observed a direct link between coalescence rate and viscositiy in crude oil [6]. In 2021, B. Bera et al. observed a positive correlation between temperature and coalescence rate, attributing this correlation to the temperature dependency of the fluid viscosity [5].

For coalescence to take place, two or more droplets of the dispersed phase have to come into close proximity. One method in which this can occur is due to creaming. Creaming occurs due to a lower density of the dispersed layer, causing the droplets to rise to the top and form a creaming layer [7]. This mechanism is explained further in 2.1.2. In recent years, much research has been done towards characterising creaming layers. In terms of experimental research, ultrasonic techniques have been used to measure oil concentration in creaming layers [8]. In more recent years, both NMR and MRI have emerged as experimental methods to characterise creaming emulsions [7]. However, due to the increasing cost and complexity of said experiments, computational methods have proven to be a powerful and efficient tool in this field. Since there is, as of yet, no single unifying theory to perfectly describe all forms of creaming behavior, it is of great importance to perform simulations using different approaches [7]. To this end, this thesis will seek to simulate the behavior of dispersed phase droplets rising towards the creaming layer. Due to previous research observing a correlation between fluid viscosity and coalescence rate, the influence of viscosity is of especial interest. As such, the main goal of this thesis will be to **determine the effects of viscosity on the rate at which creaming occurs**. To this end, this thesis will simulate the rising of an oil droplet towards a creaming layer. This is done by using the lattice Boltzmann method, which is further described in 2.2. In as early as 1993, X. Shan and H. Chen, have proposed a model within the lattice Boltzmann method to simulate the interaction force between different phases, which gives form to phase separation. This method, commonly referred to as the Shan-Chen Psuedopotential method, is further explained in 2.2.4, and will be used in this work to simulate the mechanism of creaming. To this end, S. Anwar (2013) has already made steps to simulate the rising of a gas bubble in a fluid using a similar method. This thesis seeks perform a similar research, instead focused on multicomponent systems.

This report is structured as follows: First in Chapter 2, we will explore the fundamental mechanisms of emulsions, coalescence and creaming, followed by a overview of the lattice Boltzmann method. Then in Chapter 3, the setup for the simulation will be described, along with an explanation and corresponding results of the model verification. In Chapter 4, the results yielded by the simulation will be shown and analysed. Lastly, Chapter 5 will contain a brief conclusion of the obtained results and implications, along with recommendations for future research on this topic.

2 | Theory

2.1. Emulsions

A colloid is a type of mixture in which one substance consists of microscopically dispersed particles that are suspended throughout another substance. These two phases are dubbed the dispersed phase and the continuous phase respectively [9]. An emulsion in turn is defined as a colloid in which the dispersed phase and the continuous phase are both liquids [10]. In this work, we will limit ourselves to emulsions, specifically oil-in-water emulsions, where the oil takes up the role of the dispersed phase and water that of the continuous phase.

We define two ways in which an emulsion can cease to be an emulsion. The first is called Ostwald Ripening, in which molecules of the dispersed phase present in smaller droplets slowly diffuse through the continuous phase into larger droplets. In this mechanism, the smaller oil-droplets will slowly become smaller and eventually cease to be, while the larger droplets will grow. This results in a larger average droplet size alongside a smaller total droplet count. The second method, coalescence, consists of two or more droplets of the dispersed phase coming into contact and merging, creating a single larger droplet [9]. This second mechanism will be explained in greater detail in section 2.1.1.

For coalescence to take place, oil droplets have to come into close proximity of each other. This typically happens either by creaming or aggregation [11]. In aggregation, the droplets come together due to diffusion and therefore depends on the random act of two droplets coming into contact without the presence of any attraction force. Creaming however, is the phenomenon of droplets of the dispersed phase rising to the top of the emulsion due to buoyancy effects. Since this phenomenon is the main focus of this report, it will be expanded on in section 2.1.2.

2.1.1. Coalescence

Coalescence can occur when two droplets of the dispersed phase come into close contact. Coalescence takes place in two distinct steps. The first step is a rapid thinning of the continuous phase between the two droplets, in which the continuous phase present between the two droplets is forced out due to the presence of a capillary pressure caused by the spherical shapes of the droplets. This process causes the distance between the droplets to decrease up until the system reaches a quasi-equilibrium, in which the capillary pressure has reached zero. The second step consists of a slow rupture in which the continuous phase layer still present between the droplets slowly flows out as a results of diffusion. At the end of these two steps, the droplets will come in contact, from which point coalescence can take place [12].

2.1.2. Creaming and Sedimentation

Creaming is a process in which the dispersed phase accumulates at the top of the emulsion due to buoyancy effects caused by the dispersed phase having a lower density than the continuous phase. Due to the congregation of many dispersed phase particles in a single location, particles form a creaming layer at the top of the emulsion. When a droplet comes into contact with this creaming layer, coalescence has a relatively high chance to occur due to staying in extended contact with this layer [11]. The exact composition of this creaming layer can take many different forms, including but not limited to individual droplets, partially coalesced droplets and a gel-like structure [7]. As such, there is as of yet no single theory that can predict the distribution of droplets in all types of creaming processes [7].

Since the dimensions of a given dispersed phase droplet is typically many orders of magnitude smaller than that of the distance to the creaming layer at the top of the emulsion, it can be assumed that said droplets are given enough time to reach a given "terminal velocity" v_t, for which the frictional forces F_d are equal to the buoyancy forces F_c . Due to the typically very low Reynolds number governing creaming behavior, the drag force on a dispersed phase droplet can be described by Stokes' law, which is shown in the equation below [1].

$$F_d = 6\pi\mu_c R v \tag{2.1}$$

In which R and v are the radius and velocity of the droplet respectively and μ_c is the viscosity of the continuous phase. Assuming a low enough Re, we can assume that Stokes' law is valid for a dispersed phase droplet. The buoyancy force on the droplet is given by equation (2.2).

$$F_g = \frac{4}{3}(\rho_c - \rho_d) g \pi R^3 \tag{2.2}$$

In which ρ_c and ρ_d are the density of the continuous phase and the dispersed phase respectively. The terminal velocity is reached when both forces equal each other, resulting in the following equation for v_t.

$$v_t = \frac{2}{9}\frac{(\rho_c - \rho_d)}{\mu_c} g R^2 \tag{2.3}$$

Since the time it takes for a given droplet to reach its terminal velocity is typically very small compared to the total time it takes to reach the creaming layer, it can be assumed that the droplet's average velocity can be approximated as the terminal velocity found by applying of Stokes' law.

The process of sedimentation is the opposite of creaming in that the dispersed phase is now subjected to a higher effective buoyancy force than the continuous phase, causing the dispersed phase to sink to the bottom of the emulsion [7].

2.1.3. Fluid Viscosity

The dynamic viscosity μ, generally referred to simply as "viscosity", of a liquid is a measure of its resistance to deformation. This resistance is caused by internal friction between adjacent layers of fluid that are in motion relative to each other [13]. A fluid is considered Newtonian if its viscosity is unaffected by the amount of shear stress F/A applied. In this work, we assume that all relevant components, being water and oil, are Newtonian fluids [13]. The equation for

the viscosity of a Newtonian liquid in terms of shear stress and the velocity gradient $\partial u/\partial y$ (also known as the strain rate) is given by equation (2.4).

$$\mu = \frac{F/A}{\partial u/\partial y} \tag{2.4}$$

Another form in which the viscosity can be denoted is the kinematic viscosity ν, which is defined as the ratio of the dynamic viscosity over the density of the fluid, as shown in equation (2.5) [14].

$$\nu = \frac{\mu}{\rho} \tag{2.5}$$

In the lattice Boltzmann method, this dynamic viscosity is closely related to other parameters of the simulation, and as such is typically used over the dynamic viscosity in this work. This relation is further explored in 2.2.

For a two-phase system, we also introduce a viscosity ratio η in this work, which is defined as the ratio of the kinematic viscosities of both phases as shown in equation (2.6).

$$\eta = \frac{\nu_c}{\nu_d} \tag{2.6}$$

In which ν_c and ν_d represent the kinematic viscosities of the continuous and dispersed phase respectively.

2.1.4. Interfacial Tension and Droplet Shape

Due to the strong cohesive forces between water molecules, it is more thermodynamically favorable for water molecules to neighbour each other as opposed to oil molecules. Because of this, oil molecules are effectively repelled by neighboring water molecules in a mixture that contains oil and water [15]. Due to this effective repellent force, spherical droplets are typically formed, as to decrease the contact area between the water- and oil phases, which in turn minimises the total interfacial tension between the two phases. This interfacial tension can be defined following the Young–Laplace equation, which is shown below for the case of a spherical (dispersed phase) droplet of radius R.

$$\gamma = 2\Delta p R \tag{2.7}$$

In which Δp denotes the pressure difference inside and outside of the droplet. Contrary to this phenomenon, droplets can take different shapes in the presence of external forces like gravity, or when its velocity is high enough. This shape can be described by a set of dimensionless numbers, being the Reynolds number (Re), the Bond number (Bo) and the Morton number (Mo).

The Reynolds number is the ratio of internal forces to viscous forces within a fluid and is shown in equation (2.8) for the given system. Typically, high Reynolds numbers (Re > 1000) are associated with turbulent flow, while low Reynolds numbers (Re < 1000) are associated with laminar flow [16].

$$\text{Re} = \frac{uL}{\nu_c} = \frac{2uR}{\nu_c} \tag{2.8}$$

In which u is the flow velocity, ν_c is the kinematic viscosity for the continuous phase, and L is the characteristic linear dimension of the system, which is taken as $2R$ for this work [17].
The Bond number, also called the Eötvös number, characterises the relative strength of gravity and surface tension [18] and is shown in equation (2.9).

$$\text{Bo} = \frac{gR^2(\rho_c - \rho_d)}{\gamma} \tag{2.9}$$

In which g is the acceleration due to gravity. A high Bond number designates that the gravity forces are dominating over the surface tension, typically resulting in a deformation of the droplet. The Bond number is used to describe the overall shape of the droplet together with the Morton number, which is shown in equation (2.10).

$$\text{Mo} = \frac{g{\nu_c}^4{\rho_c}^2(\rho_c - \rho_d)}{\gamma^3} \tag{2.10}$$

Similar to the Bond number, the Morton number is used to characterise the deformation for a droplet rising in a liquid due to buoyancy effects. Contrary to the Bond number, the Morton number is not dependent on R, and is therefore consistent for droplets that vary in size. A high Morton number is associated with a high degree of deformation of the droplet.

2.2. The Lattice Boltzmann Method

The lattice Boltzmann method is a Computational fluid dynamics (CFD) method, used in the simulation of fluid behavior. Contrary to other many other CFD methods, the lattice Boltzmann method does not solve the Navier Stokes Equations directly [18]. Instead, a lattice is simulated, for which each node is assigned a fluid density function which contains information about the density and overall velocities of particles at the given node. For every time step in the simulation, the overall velocity at each node is re-evaluated using a collision operator, simulating collisions of particles in addition to other applied forces. Afterwards, a streaming step is performed in accordance with the assigned velocities. Both steps in this process are described in greater detail in their corresponding sections.

2.2.1. The Particle Distribution Function

The most integral variable in the lattice Boltzmann method is the particle distribution function $f(\vec{x}, \vec{\xi}, t)$, which designates for a given point $\vec{x}$ how many particles (in terms of mass density) will have velocity $\vec{\xi}$ at time t. To simplify this variable, the velocity space is discretised. This is done by declaring that for $\vec{\xi}$, only a finite number of values $\vec{c_i}$ are possible. Since this work is exclusively simulating a 2D system, we will limit ourselves to the use of the D2Q9 velocity set, in which the 2 designates the number of dimensions and 9 represents the amount of possible values for $\vec{c_i}$ [18]. Each of the velocities $\vec{c_i}$ have a weighting coefficient w_i associated with them, which directly influences the chance for a given particle to have said velocity. The 0th term represents the rest velocity, in which a particle does not move and hence $\vec{c_0} = \vec{0}$. It has $w_0 = \frac{4}{9}$. Terms 1 to 4 represent movement along a Cartesian axis and have $w_i = \frac{1}{9}$. Terms 5 to 8 represent movement with a $45°$ angle with either of the Cartesian axes and have $w_i = \frac{1}{36}$. The magnitude of said velocities are defined such that in a given time step Δt, the corresponding

populations move either a single node in the case of $i \in 1, 2, 3, 4$ or diagonally in the case of $i \in 5, 6, 7, 8$ for a total magnitude of $|\vec{c_i}| = \sqrt{2}$. This discretisation scheme is also shown in the figure below.

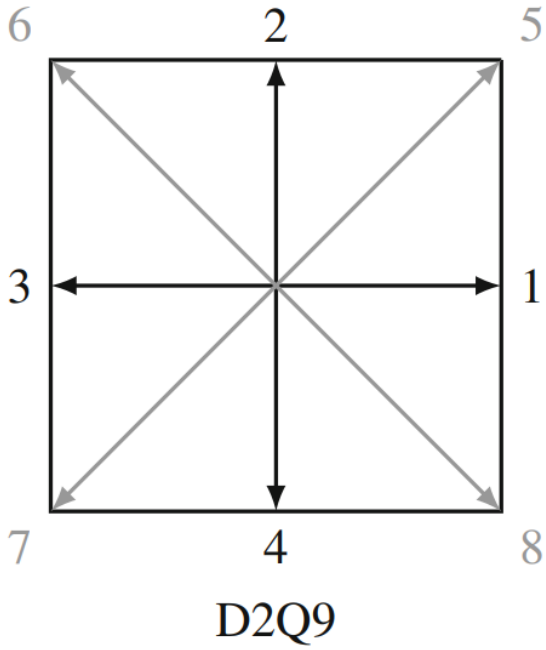

Figure 2.2.1: Here the possible directions are shown for the D2Q9 discretisation scheme. Velocities with length $|\vec{c_i}|$ = 1 and $\sqrt{2}$ are shown in black and grey, respectively. Note that the rest velocity $\vec{c_0} = \vec{0}$ is not shown [18].

With this discretised velocity scheme, we can redefine the particle distribution function as $f_i(\vec{x}, t)$, where i designates the corresponding velocity in accordance with the D2Q9 scheme. Using this scheme, we can calculate the following quantities on each given node.

$$\textbf{Density:} \quad \rho(\vec{x}, t) = \sum_i f_i(\vec{x}, t) \tag{2.11}$$

$$\textbf{Velocity:} \quad \vec{u}(\vec{x}, t) = \sum_i \frac{\vec{c_i} f_i(\vec{x}, t)}{\rho(\vec{x}, t)} \tag{2.12}$$

2.2.2. Collision Step

At every time step, the populations at each node are reconfigured, as to come closer to a equilibrium population $f_i^{eq}(\vec{x}, t)$. This equilibrium population is calculated using the following equation:

$$f_i^{eq}(\vec{x}, t) = w_i \rho(\vec{x}, t)(1 + \frac{\vec{u} \cdot \vec{c_i}}{c_s} + \frac{(\vec{u} \cdot \vec{c_i})^2}{2c_s^4} - \frac{\vec{u} \cdot \vec{u}}{2c_s^2}) \tag{2.13}$$

In which c_s is the speed of sound, which gives a measure of how fast information can propagate through the system. In the lattice Boltzmann method, the speed of sound equals $c_s = \frac{1}{\sqrt{3}} \frac{lu}{tu}$, in

which lu and tu (commonly referred to as lattice units) are the resolutions of the grid in terms of space and time respectively [19]. Another lattice unit is mu, which denotes mass. Using this equilibrium population, we define an operation to determine how much closer the population at the given node will be to this equilibrium population after a given time step Δt. This is done by using the Bhatnagar-Gross-Krook (BGK) operator, Ω_i, which is calculated using equation (2.14).

$$\Omega_i(\vec{x}, t) = -\frac{f_i(\vec{x}, t) - f_i^{eq}(\vec{x}, t)}{\tau} \tag{2.14}$$

In which the relaxation time τ is a variable which directly influences the how quickly a population will reach its corresponding equilibrium population. In terms of physical properties, τ is directly related to the kinematic viscosity υ as shown in equation (2.15).

$$\upsilon = c_s^2(\tau - \frac{\Delta t}{2}) \tag{2.15}$$

Using the BGK-operator, the population for every time step is restructured as follows.

$$f_i(\vec{x}, t + \Delta t) = f_i(\vec{x}, t) + \Omega_i(\vec{x}, t) \tag{2.16}$$

2.2.3. Streaming Step and Boundary Conditions

The second step in the process is the streaming step, in which populations with velocity $\vec{c_i}$ will propagate from a position $\vec{x}$ to $\vec{x}$ + $\vec{c_i}$. This process can be seen in the equation below.

$$f_i(\vec{x} + \vec{c_i}\Delta t, t + \Delta t) = f_i(\vec{x}, t) \tag{2.17}$$

Since this simulation will take place in a finite grid, boundary conditions have to be defined, as to conserve mass for the system. The two boundary conditions that will be considered in this work are periodic boundary conditions and bounce-back boundary conditions. Periodic boundary conditions rest on the key assumption that the system, both in terms of flow and geometry, are periodic, in the sense that each grid of identical size will be the same in terms of flow and component density. The application of this boundary condition in the simulation rest on that if a population is about to exit the grid on one side, they will re-enter from the other side. In a 2D $N_x \times N_y$ grid with periodic boundaries at $x = 0$ and $x = N_x$, we attain the following equations.

$$f_i(0, y_2, t + \Delta t) = f_i(N_x - 1, y_1, t) \quad |\vec{c_i} \cdot \hat{x} = 1 \tag{2.18}$$

$$f_i(N_x - 1, y_2, t + \Delta t) = f_i(0, y_1, t) \quad |\vec{c_i} \cdot \hat{x} = -1 \tag{2.19}$$

With $\hat{x}$ denoting the unit vector in the x-direction. Not to be confused with the position $\vec{x}$.

When using bounce-back boundary conditions on the other hand, we define both sides of a grid as solid walls, through which no population can propagate. When implemented in the Lattice Boltzmann method, it results in a population that is about to exit the grid to invert their respective velocity, resulting in an elastic collision. For a bounce-back boundary condition for $y = 0$ and $y = N_y + 1$, the resulting velocity shift of populations approaching the $y = N_y + 1$ boundary is shown in the equations below.

$$\begin{aligned} f_4(x_2, N_y, t + \Delta t) &= f_2(x_1, N_y, t) \\ f_7(x_2, N_y, t + \Delta t) &= f_5(x_1, N_y, t) \\ f_8(x_2, N_y, t + \Delta t) &= f_6(x_1, N_y, t) \end{aligned} \tag{2.20}$$

For populations approaching the $y = 0$ boundary, the below equations are given.

$$\begin{aligned} f_2(x_2, 1, t + \Delta t) &= f_4(x_1, 1, t) \\ f_5(x_2, 1, t + \Delta t) &= f_7(x_1, 1, t) \\ f_6(x_2, 1, t + \Delta t) &= f_8(x_1, 1, t) \end{aligned} \tag{2.21}$$

2.2.4. Multi-component Systems & Shan Chen forcing

Introducing forces to the simulation in this work is done by the velocity shifting method, proposed in the original works of Shan and Chen (1993), in which a forcing term is added to the velocity used in calculating the equilibrium population in equation (2.13) [20]. To implement this, a new variable, denoted by the equilibrium velocity, is introduced, which is shown in the equation below.

$$\vec{u}^{eq}(\vec{x}, t) = \vec{u}(\vec{x}, t) + \frac{\tau \vec{F}(\vec{x}, t) \Delta t^2}{\rho(\vec{x}, t)} \tag{2.22}$$

In the case of multiple components (for example water and oil) being simulated, all populations have to be labeled by a superscript σ, which denotes said component[1]. For this case, we define a weighted average of velocities, which we denote the common velocity $\vec{u}'$, for which the following relation holds.

$$\vec{u}'(\vec{x}, t) = \sum_{\sigma} \frac{\rho^{(\sigma)}(\vec{x}, t) \vec{u}^{(\sigma)}(\vec{x}, t)}{\tau^{(\sigma)}} \left(\sum_{\sigma} \frac{\rho^{(\sigma)}(\vec{x}, t)}{\tau^{(\sigma)}} \right)^{-1} \tag{2.23}$$

This newly defined common velocity is used instead of the single-component velocity in the calculation of $\vec{u}^{eq}(\vec{x}, t)$ in equation (2.22).

[1]Note that when talking in Lattice Boltzmann terms, the term "phase" usually refers to a state of matter (i.e. gas or liquid), whereas in this work and emulsion science in general, "phase" also refers to different immiscible components (i.e. water and oil). To avoid confusion, in this subchapter the word "component" is used when referring to a substance. Since an emulsion by definition consists of multiple components and a single state of matter (liquid), in this work the term "phase" is reserved for components unless otherwise mentioned.

The gravity force in this work is introduced following equation (2.24).

$$F_g{}^{(\sigma)} = -g\frac{\rho^{(\sigma)}}{\sum_\sigma \rho^{(\sigma)}}(\rho^{(\sigma)} - \rho_0) \tag{2.24}$$

In which ρ_0 is a reference density equal to the density of water, which is taken at unity. For this work, to simulate a system where the dispersed phase has a constant density, a Boussinesq approximation is applied in which the density for the oil component is taken as its base density in the second term. This approximation ensures that despite unwanted density variations inside the simulation, the buoyancy force works as if the oil phase has a fixed density [18].

To simulate interfacial tension, the Shan-Chen Pseudopotential Method is used. This method, proposed by X. Shan and H. Chen (1993), rests on the assumption that for every node, a force acts on the populations of component σ that is dependent on the population of all components $\tilde{\sigma}$ in adjacent nodes. This force is dependant on pseudopotential $\psi^{(\sigma)}$. Due to this work using relatively low density ratios between components, the pseudopotential is taken simply as ρ, as shown in equation (2.25).

$$\psi^{(\sigma)} = \rho^{(\sigma)} \tag{2.25}$$

In other works, particularly those with with high density ratios such as multiphase systems, other, more elaborate definitions for ψ are used [18]. The Shan-Chen force on the population of a component σ on a given node $\vec{x}$ is calculated using equation (2.26).

$$\vec{F}^{SC(\sigma)}(\vec{x}) = -\psi^{(\sigma)}(\vec{x})\sum_{\tilde{\sigma}} G_{\sigma\tilde{\sigma}} \sum_i w_i \psi^{(\tilde{\sigma})}(\vec{x} + \vec{c_i}\Delta t)\vec{c_i}\Delta t \tag{2.26}$$

In which $G_{\sigma\tilde{\sigma}}$ denotes a coefficient which denotes the interaction strength between liquids σ and $\tilde{\sigma}$, refered to as the interaction parameter. For a positive value, the two components will repel each other, and for a negative value the two components will attract each other. The equation of state for the multicomponent SC model as used in this work is given by equation (2.27) [21].

$$p = \sum_\sigma {c_s}^2 \rho^{(\sigma)} + \frac{{c_s}^2 \Delta t^2}{2} \sum_{\sigma,\tilde{\sigma}} G_{\sigma\tilde{\sigma}} \psi^{(\sigma)} \psi^{(\tilde{\sigma})} \tag{2.27}$$

In this work, we always assume that $G_{\sigma\tilde{\sigma}}$ is only nonzero for $\sigma \neq \tilde{\sigma}$, resulting in the Shan-Chen force only being applied between different components. Since there are only two components, we will refer to the interaction strength between water and oil simply as G.

2.3. Literature Review

In the past years, the lattice Boltzmann method has been a popular research tool for multiphase and multicomponent systems like emulsions. In 1993, X, Shan and H. Chen devised a method for simulating flows with multiple phases and components, colloquially known as the Shan-Chen model. This method is still popular for lattice Boltzmann simulations that rest on phase or component separation due to its simplicity and mesoscopic nature [18]. In 2012, S. Gong and P. Cheng have used multiple forms of the Shan-Chen method to simulate a liquid droplet in a vapor. These results were compared against theoretical values and yielded satisfactory results. In the same work, the coalescence of two droplets along a solid surface in a 3D space is simulated for which the results are shown in figure 2.3.1.

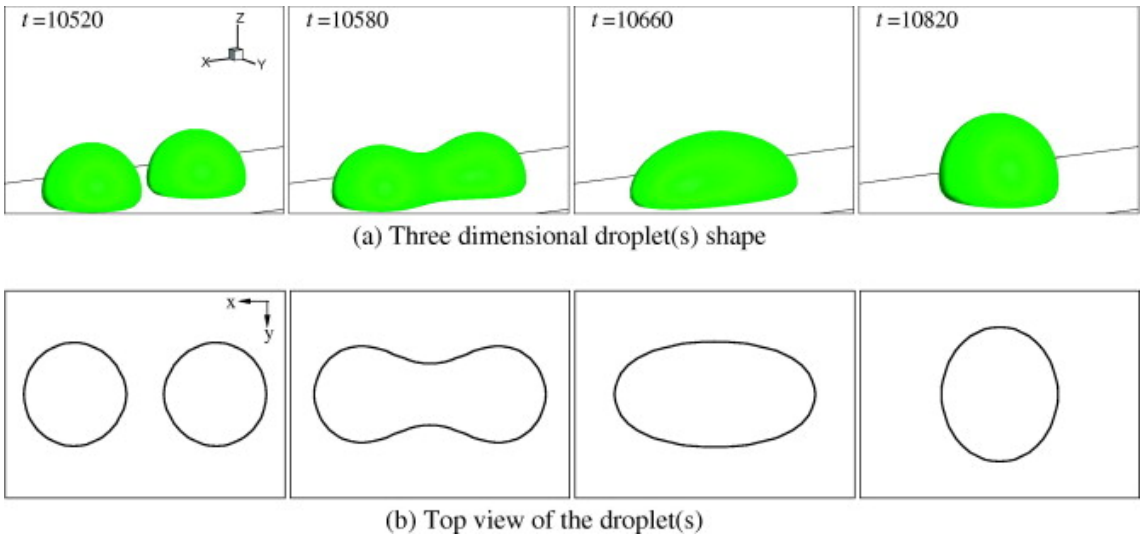

(a) Three dimensional droplet(s) shape

(b) Top view of the droplet(s)

Figure 2.3.1: Coalescence of two droplets on the bottom surface with wettability gradients in a microchannel, as simulated by S. Gong and P. Cheng. Both a side-view and top-down view is given in the first and second set of images respectively. Each set of images is linked to a different time value t and represents a corresponding step in the coalescence progress [22].

From their results, Gong and Chenq concluded that their application of the lattice Boltzmann method is "an effective tool for simulations of phase transitions and multiphase flows" and that more complex fluid problems can also be analysed using this method [22].

In 2013, S. Anwar used a modified version of Gunstensen's binary color model in the lattice Boltzmann method to simulate gas bubbles rising in a liquid due to buoyancy effects. By varying the viscosity of the present phases, he found that the terminal velocity is positively correlated to the viscosity ratio η for values of $\eta < 500$, as shown in Figure 2.3.2.

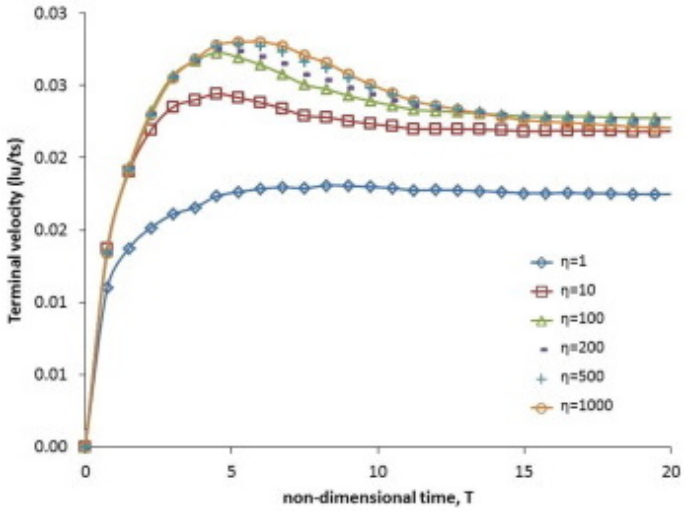

Figure 2.3.2: S. Anwar's results for the terminal velocity of a gas bubble rising in a liquid due to buoyancy effects for various viscosity ratios. On the y-axis the terminal velocity of the droplet is shown, and on the x-axis the corresponding non-dimensionalised time $T = \Delta t\sqrt{g/2R}$ is shown. This plot contains graphs for multiple viscosity ratios ranging from $\eta = 1$ to $\eta = 1000$ [19].

S. Anwar also observed that for a lower viscosity ratio, the bubble suffers less deformation. In the same work, he also observed that a high Bond number relates to a lower surface tension, which in turn causes higher bubble deformation. Lastly, Anwar compared the shape of the resulting bubbles for varying values for Bo and Mo to experimental data provided by Bhaga and Weber [23]. He concluded that the resulting shapes are in agreement with said experimental data and his results serve as a verification of an LBM-based buoyant multiphase flow model to simulate density dependent flow of a binary mixture of fluids.

3 | Numerical Method

In this work the research question has been addressed using the lattice Boltzmann method with the help of a newly written Python script. This simulation will take place on a 2D $N_x \times N_y$ grid and will use the D2Q9 velocity scheme, as explained in 2.2.1. The simulated system mimics an oil-in-water emulsion, where the two components are given by oil as the dispersed phase with a density of $0.8\,mu/lu^2$ and water as the continuous phase with a density of $1\,mu/lu^2$. In this work, the Shan-Chen method is used with an interaction parameter of $G = 2.5$, which is found to cause less diffusion for higher values of τ, while still ensuring stability of the system.

A limitation of the Lattice Boltzmann method lies in the choice for the relaxation time τ, and therefore the kinematic viscosity ν. In general, a low relaxation time ($\tau < 0.6\Delta t$) will often result in instabilities [18], whereas a high relaxation time ($\tau >> 1\Delta t$), will result in a lower accuracy for the results [24]. In this work we will limit ourselves to $0.7\Delta t \leq \tau_c \leq 3\Delta t$ and $0.8\Delta t \leq \tau_d \leq 1.4\Delta t$ for the relaxation parameters for the continuous phase and dispersed phase respectively.

3.1. Model Validation

To validate the proposed model, a test is performed to see if the system follows the Laplace law, given by equation (2.7). To test this, this work will follow similar steps as S. Nekoeian et al. (2018), in which oil-phase square of width d_0 is placed in the center of a $100\,lu$ by $100\,lu$ grid [25]. The rest of the grid is filled with water-phase. The relaxation time for both components is set at $1\Delta t$. Afterwards, the system is set to equilibriate for $5000\,\Delta t$. This is done for multiple values of d_0, ranging from $d_0 = 8\,lu$ to $d_0 = 40\,lu$. As seen in the figure below, in accordance with the theory explored in 2.1.4, the oil-phase will gradually take the shape of a circle, as to minimize interfacial tension.

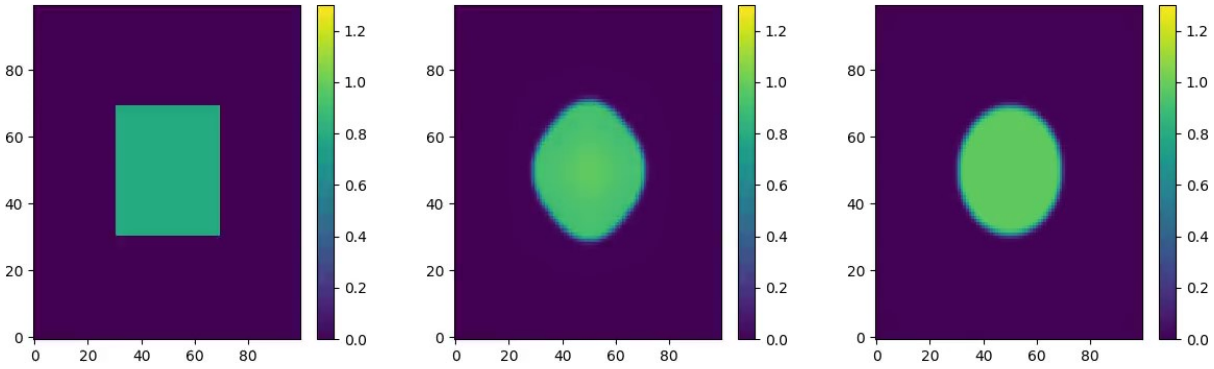

(a) $t = 0\,\Delta t$ (b) $t = 200\,\Delta t$ (c) $t = 5000\,\Delta t$

Figure 3.1.1: Here the oil phase for the droplet test for $d_0 = 40\,lu$ is visualised. The x- and y-axes denote the respective coordinates and the color represents the density of the oil phase. The water phase is not visualised in this figure. The three figures show the oil phase at $t = 0\,\Delta t$, $t = 200\,\Delta t$ and $t = 5000\,\Delta t$ respectively. Note that as t increases, the oil phase approaches the shape of a circle.

According to Laplace's Law shown in equation (2.7), the pressure difference at the interface of a given droplet is inversely proportional to its radius for a given γ. By using equation (2.27), this pressure is calculated for each of the given starting diameters. This is done by letting the system equilibriate for $5000\,\Delta t$, after which the pressure p is calculated for every x for $y = \frac{1}{2}Ny = 50$. Next p is compared between the center of the droplet (given as $x = \frac{1}{2}Nx = 50$) and just outside of the droplet. Since the radius R of the droplet varies with d_0, this value for x (and in the same sense the value for R) has to be picked by hand. In the figure below, the pressure difference Δp is plotted against $\frac{1}{R}$.

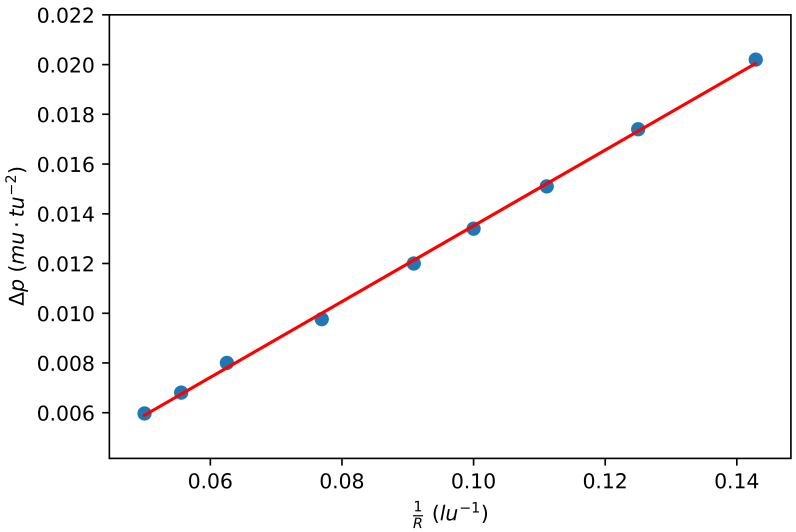

Figure 3.1.2: The value of $\frac{1}{R}$ is plotted against Δp. All values are in Lattice Boltzmann Units. The dots represent the measurements, whereas the line is curve fit with values 0.152 and -0.0017 for the slope and starting y-value respectively.

As can be seen from the results of this validation, Δp is indeed linear with $\frac{1}{R}$. Following Laplace's Law, this indicates that γ is constant for all values of R for a constant G. Using the values of the curve fit, γ is found at $0.152\,mu\,lu\,tu^{-2}$.

3.2. Buoyancy Effects

A circular oil droplet with radius $R_0 = 12\,lu$, is initialized in the center of a grid with dimensions of $8\,R_0$ and $12\,R_0$ for the x- and y axes respectively. This grid is defined as to minimize wall effects and improved accuracy in accordance with the steps taken by S. Anwar (2013). The rest of the grid is populated with water. A time T_0 after initializing, a gravitational constant of $g = 0.005$ is introduced as shown in equation (2.24). This waiting period is taken at $T_0 = 1000\Delta t$, as to give the initial system time to equilibrate [26]. Next, after initialising the gravitational force, the average y-velocity of the oil population is tracked as a function of time. The system is given another $500\,tu$ for the droplet to reach its terminal velocity. Next, to minimize the effects of fluctuations in the obtained terminal velocity, it is taken as an average over another $300\,tu$. This value is denoted by the terminal velocity v_t. This process is done for $\tau_c \in \{0.7, 0.8, 1, 1.4, 2.5, 3\}$ and $\tau_d \in \{0.8, 1, 1.4\}$. The results are presented in chapter 4.

4 | Results and Discussion

In this chapter, the results for the lattice Boltzmann method simulation for buoyancy effects in an emulsion proposed in chapter 3 will be presented and discussed.

4.1. Buoyancy Driven Creaming Behavior

The rising of a dispersed phase droplet in an oil-in-water emulsion due to buoyancy effects was simulated. This rising is quantified by v_t, for which the found values are shown in Figure 4.1.1 for each combination of relaxation parameters τ_d and τ_c.

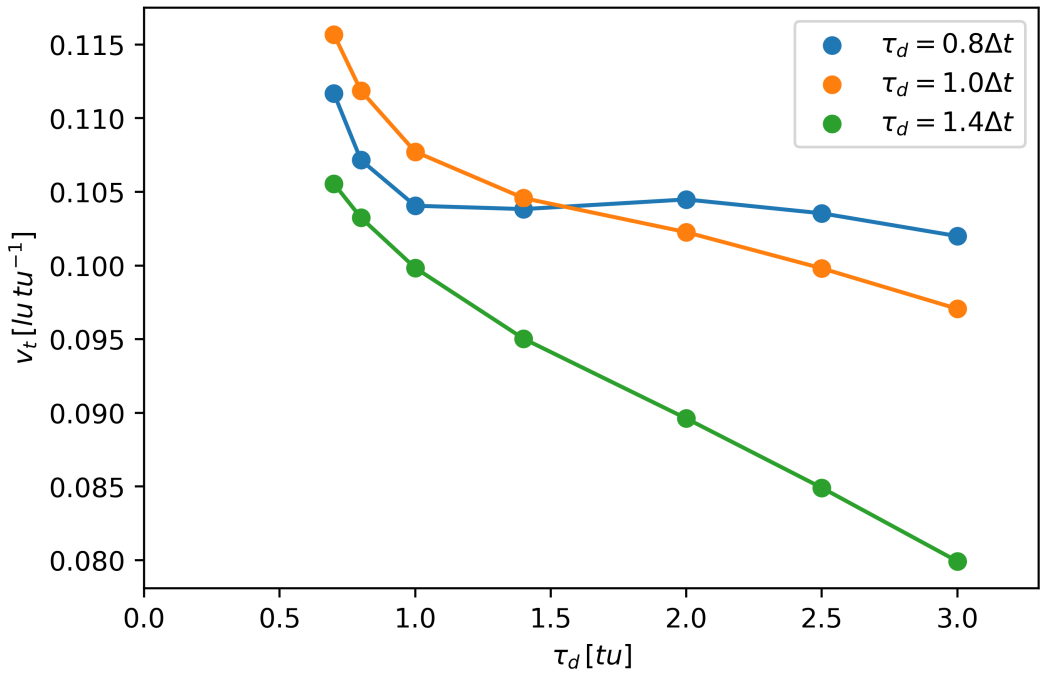

Figure 4.1.1: The results for the described measurements. The calculated terminal velocities v_t are shown on the y-axis in $lu\,tu^{-1}$ and plotted against the relaxation parameter of the continuous phase τ_c in tu. This is done for three values of τ_d, as presented by the legend found in the upper right corner of the figure.

As can be seen from Figure 4.1.1, the terminal velocity decreases as the relaxation parameter increases for the given ranges. Since the relaxation parameter of a given component

is linearly related to said component's viscosity, this confirms a negative correlation between terminal velocity and viscosity for the given system.

Equation (2.3) gives an estimation for the relation between v_t and ν_c. To see whether this relation holds for the given simulations, in Figure 4.1.2 the obtained terminal velocities are plotted against the corresponding continuous phase kinematic viscosity.

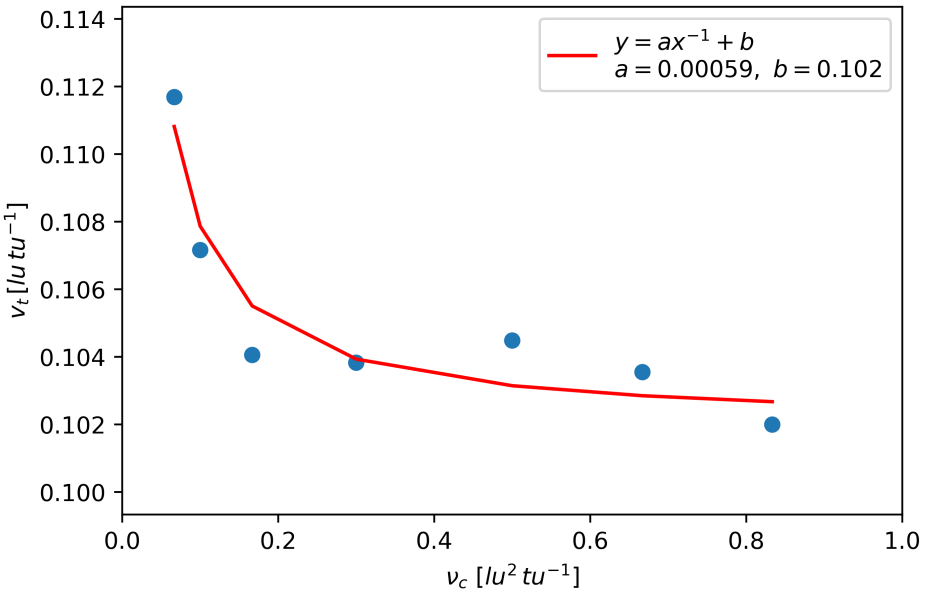

(a) $\tau_d = 0.8\,\Delta t$

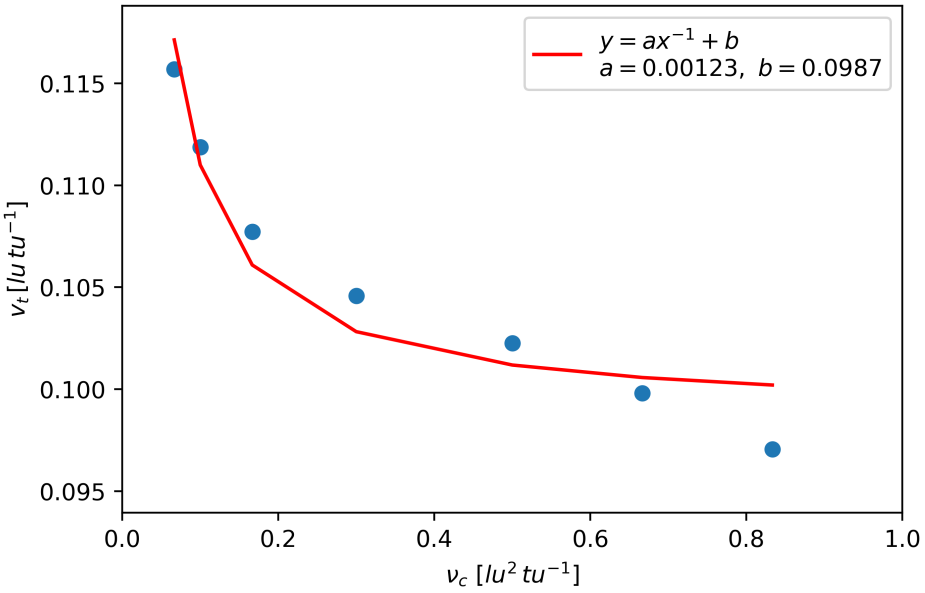

(b) $\tau_d = 1.0\,\Delta t$

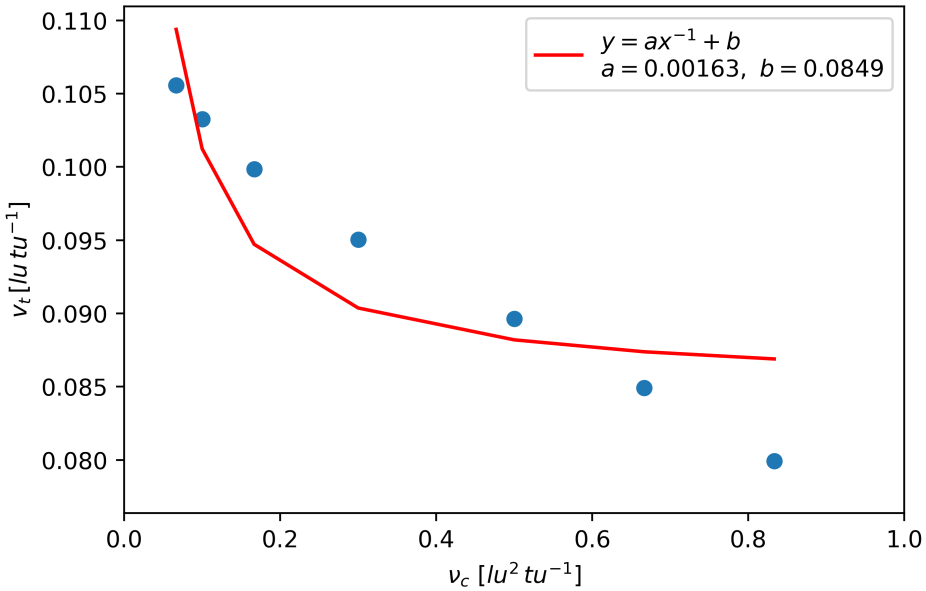

(c) $\tau_d = 1.4\,\Delta t$

Figure 4.1.2: The results for the given measurements. The calculated terminal velocities v_t are shown on the y-axis in $lu\,tu^{-1}$ and plotted against the kinematic viscosity of the continuous phase ν_c, which is shown on the x-axis. Plot (a), (b) and (c) respectively show results for a dispersed phase relaxation parameter of $\tau_d = 0.8\Delta t$, $\tau_d = 1\Delta t$ and $\tau_d = 1.4\Delta t$. The blue dots represent calculated simulation results. The red curve represents an inverse curve fit for each of the given values for τ_d, for which the value is shown in the upper right corner of the respective graph.

As seen in figure 4.1.2, the terminal velocities for the given parameters tend to decrease as the viscosity of the continuous phase increases. The obtained results do not follow an inverse relation, which contradicts results expected from equation (2.3). The results seem to follow an inverse proportionality more closely for lower values of τ_d, which can possibly be attributed to a lesser amount of droplet radius fluctuations, as can be seen in Figure 4.2.1 and Figure 4.2.2. Equation (2.3) however predicts a direct inverse proportionality between ν_c and v_t, which is not present in the obtained results.

To test whether the terminal velocity is dependant on the viscosity ratio, the figure below shows said terminal velocities plotted against η as opposed to ν_c

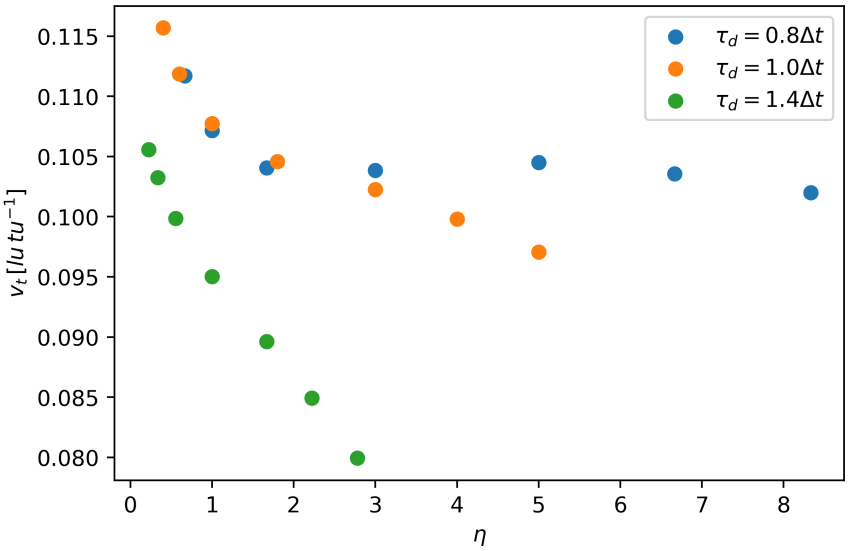

Figure 4.1.3: The obtained values for v_t are plotted on the y-axis in $lu\, tu^{-1}$ against η on the x-axis. The three colours represent results for different values for τ_d, as can be seen from the label in the top right of the graph.

Results obtained from a similar simulation performed by S. Anwar (2013), presented in Figure 4.1.4, show a positive correlation between viscosity ratio η and the terminal velocity v_t. As can be seen from Figure 4.1.3, no correlation can be found between said variables. Multiple obtained values for v_t for the same value of η indicate that v_t is not solely dependant on η.

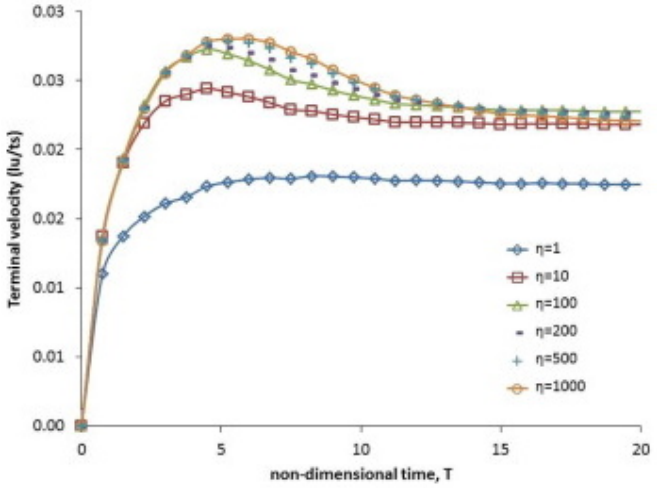

Figure 4.1.4: S. Anwar's results for the terminal velocity of a gas bubble rising in a liquid due to buoyancy effects for various viscosity ratios. On the y-axis the terminal velocity of the droplet is shown, and on the x-axis the corresponding non-dimensionalised time $T = \Delta t\sqrt{g/2R}$ is shown. This plot contains graphs for multiple viscosity ratios ranging from $\eta = 1$ to $\eta = 1000$ [19].

4.2. Discussion

The calculated values for v_t do not directly follow the inverse proportionality predicted by equation (2.3). Multiple explanations are given for this discrepancy. The first explanation is that Stokes' law is only applicable to flow governed by a low Reynolds number (Re < 1). An estimation for the Reynolds number in the given simulation is found to vary between 3 and 30, depending on ν_c. As a result, the simulated flow is not adequately described by Stokes' law. A possible solution for further simulations for describing creaming behavior is to use use lower values of g, as to better describe the low speed, and therefore Reynolds number, governing creaming behavior.

Another likely factor that attributes to v_t and ν_c not following an inverse proportionality is the dependency on R^2 in Stokes' law. While the initial diameter of the droplet in each simulation is fixed, the variations in viscosity yield slightly different diameters for the droplets after equilibrating. This can be attributed to two factors, being dispersion and density fluctuations. Dispersion of the droplet is caused by an insufficient value for the surface tension γ. As can be seen in Figure (4.2.1), diffusion can be found to be especially prevalent for high values of τ_d, and prevents the model used in this work from being used for values of $\tau_d > 1.4$ as the droplet diameter reaches values too close to the grid resolution, resulting in inaccurate results. Fluctuations of density in the oil-phase present in the droplet are caused by an excess or lack of surface tension. A known limitation for the velocity shift forcing approach used in this work is a τ-dependant surface tension, which is an non-physical effect [18]. As can be seen in Figure (4.2.1), the density inside the droplet can be found to increase with τ_d and decrease with τ_c. In further works on this subject, another force implementation method should be used as to attain a fixed value for γ for all values of τ. A multiple-relaxation-time lattice model proposed by Z. Chai and T. Zhao (2012) has shown to yield accurate results with differing viscosity values between components. Another possible solution for the unwanted density fluctuation would be to vary the initial diameter or density distribution of the initialised droplet, as to find a combination of initial parameters for each set of viscosities that results in the desired droplet composition after equilibrating. This method however can prove to be very resource intensive, as these parameters have to be found for each set of viscosities. Since this approach is beyond the scope of this work, a Boussinesq approximation has been used for the gravity force applied to the oil phase, which accounts for the variation in density, but not for the variation in droplet radius. The droplet shape and densities right before applying gravity forces are shown in Figure (4.2.1).

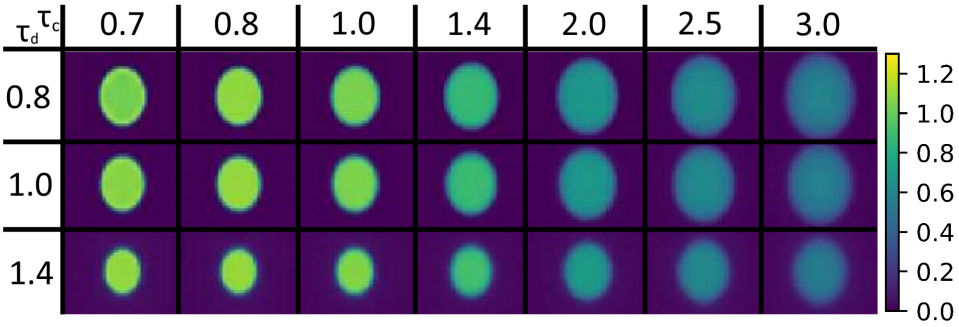

Figure 4.2.1: Here the oil phase right before applying gravity is visualised. As can be seen on the bar on the right of the figure, brighter colours represent higher densities, whereas darker colours represent lower densities. From left to right, the droplets correspond to simulations with increasing values of τ_c and from top to bottom with increasing values of τ_d. Note that as τ_d increases, the droplet diameter decreases despite no visual increase in density, indicating a loss of mass due to diffusion. Also note that as τ_c increases, the droplet diameter increases whereas the density inside the droplet decreases.

The second factor for the droplet not following equation (2.3) is that Stokes' law assumes a perfectly spherical droplet. As is confirmed by both experimental and numerical research, a large Bond number causes droplet deformation, resulting in a non-round shape [23] [19]. An estimate value for the Bond number in the given simulations is found as 1, varying with γ. Since the Morton number is highly dependant on γ, which is not known, a reasonable estimate cannot be given. As can be seen in Figure 4.2.2, droplet deformation is especially prevalent for higher values of τ_c. This result indicates that Stokes' law is not applicable to creaming behavior governed by a high Bond number. Future research could be done with lower values for g, as to see if the corresponding results follow equation (2.3) more closely.

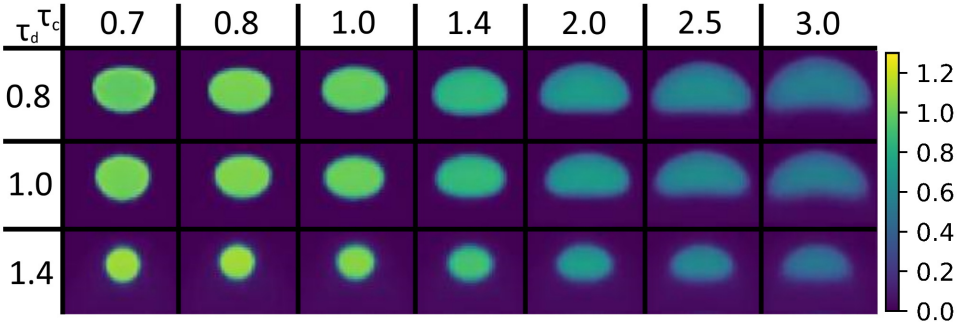

Figure 4.2.2: Here the oil phase at $800\,tu$ after initialising the gravity forces is visualised. As can be seen on the bar on the right of the figure, brighter colours represent higher densities, whereas darker colours represent lower densities. From left to right, the droplets correspond to simulations with increasing values of τ_c and from top to bottom with increasing values of τ_d. Note that as τ_c increases and τ_d decreases, droplet deformation starts to occur, resulting in deviations from the original round droplet. Note that, as in Figure 4.2.1 diffusion and density fluctuations can be observed for varying values for τ_d and τ_c.

Lastly, the terminal velocity of a given droplet has to be estimated as an average over a limited period of $300\,tu$. Despite the droplet theoretically achieving a fixed velocity, the tracked velocity in practice tends to oscillate as seen in Figure 4.2.3. These fluctuations can be attributed to many effects including but not limited to spurious currents, wall effects, density fluctuations, gradual shape deformation and dispersion.

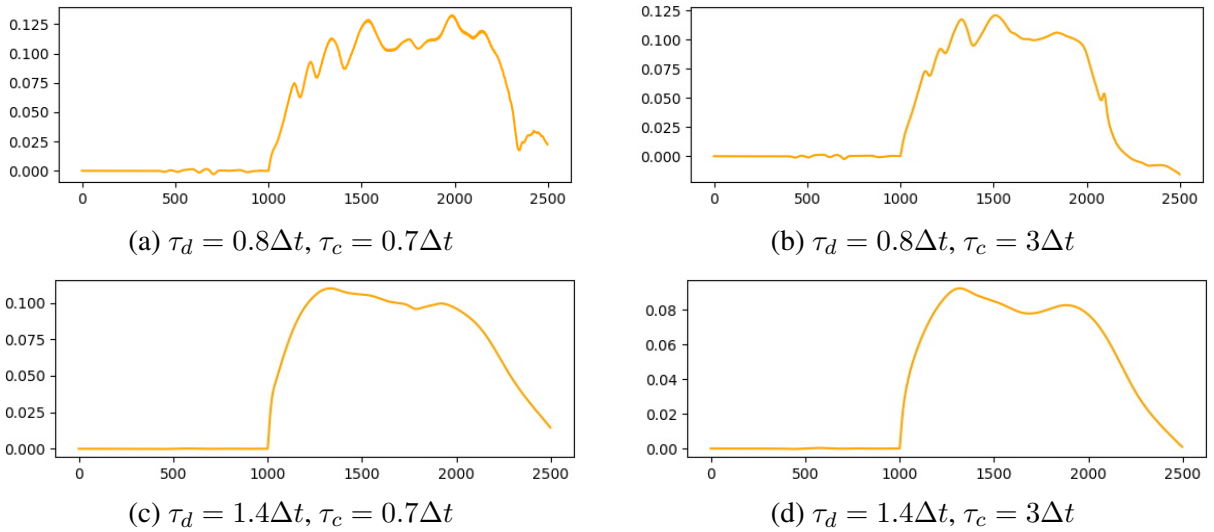

(a) $\tau_d = 0.8\Delta t$, $\tau_c = 0.7\Delta t$

(b) $\tau_d = 0.8\Delta t$, $\tau_c = 3\Delta t$

(c) $\tau_d = 1.4\Delta t$, $\tau_c = 0.7\Delta t$

(d) $\tau_d = 1.4\Delta t$, $\tau_c = 3\Delta t$

Figure 4.2.3: The obtained overall velocity of the dispersed phase in the y-direction for different sets of τ. On the y-axis, the average y-velocity of the dispersed phase is shown in $lu\,tu^{-1}$. On the x-axis, the total time that has passed since the beginning of the simulation is shown. At time $t = 1000\,tu$, the gravitational force is introduced. v_t is taken as an average from $t = 1500\,tu$ to $t = 1800\,tu$.

As can be seen from Figure 4.2.3, the velocity fluctuations vary in scale and frequency for different viscosity values, seemingly becoming more stable for higher values for τ_d. Note that for higher values for t, the velocity starts to decrease, as this is when the droplet starts to come close to the top of the grid, and starts being affected by wall effects, limiting the time range over which v_t can be averaged to a $300\,tu$. In future research, the time over which the terminal velocity is averaged can be extended by either increasing the grid size in the y-direction or lowering the terminal velocity by using a lower value for g.

No correlation was found between the terminal velocity v_t and the viscosity ratio η. Similar simulations done by S. Anwar (2013) have however shown a positive correlation between said variables. This discrepancy is most easily explained by the difference in subject matter being simulated. Since S. Anwar's model simulates a multiphase system with high density density ratio, as opposed to a multicomponent system with a low density ratio, the two cases can yield different results, despite being based on the same principle.

5 | Conclusion

In this work, the creaming behavior of an oil-in-water emulsion has been simulated using the lattice Boltzmann method. This is done by implementing the Shan-Chen pseudopotential method for a multicomponent system. Gravity forces were applied on a dispersed phase droplet with an initial radius R, after which a terminal velocity v_t is found, which is used to quantify the rate at which creaming occurs for the given parameters. This is done for independently varied viscosities for both the dispersed phase and continuous phase, denoted by ν_d and ν_c respectively. A negative correlation was observed between v_t and ν_c, which becomes stronger for higher values for ν_d. The results were compared to theoretical predictions for v_t based on Stokes' law and were found not to follow an inverse relation between v_t and ν_c as expected for creaming behavior [1]. A high Reynolds number, variations in droplet diameter, variations in density, droplet deformation and velocity fluctuations are factors that can attribute to this discrepancy. The terminal velocity v_t was also compared to viscosity ratio η, but no direct dependency between the two variables was found. This contradicts results for similar multiphase simulations performed by S. Anwar (2013), although this discrepancy can be explained by differences in simulation parameters like density ratio.

5.1. Recommendations

This work can be used as a baseline towards future simulations of creaming behavior using the lattice Boltzmann method. Since the obtained results are not fully in line with theoretical predictions, the primary focus of future simulations should be to attain results that better reflect actual creaming behavior, for which recommendations are listed below.

- It is recommended to lower the gravity constant g as to better reflect the slow movement associated with creaming and lowering the turbulence, yielding results more in line with predictions based on Stokes' law. This lowering of overall velocity also lowers the dimensionless Bond number and Morton number, which both quantify the deformation of said droplet due to gravity, resulting in a lower degree of droplet deformation.
- It it also recommended for the averaging of v_t to take place over a large time range. To achieve this however, a larger grid must be used as to lessen the wall effects present when the droplet approaches the upper boundary of the grid, increasing computation time.
- A limitation present in the current simulation is that the surface tension is dependent on the chosen relaxation parameters, and are therefore directly linked to the viscosities. To eliminate this dependency, another forcing scheme will have to be used as opposed to the velocity shift method, for which multiple have been proposed [26] [27].
- Droplet density fluctuations will have to be lessened as to attain a stable value for R. This can possibly done by initialising each droplet with a set of initial parameters that ensure stability for the simulated droplet.

In addition to obtaining better results, future simulations can also be done extending the scope of this work. Some recommendations are listed below.

- Future simulations can be done on larger ranges of ν_c and ν_d to see whether an inverse relation for v_t and ν_c is found for lower or higher viscosity values of either phase. Using a different forcing scheme which yields stable results for high viscosities will expand the range of simulations that can be performed using this method [27].
- Droplet deformation under buoyancy effects can also be further quantified using dimensionless numbers Bo and Mo and a relation between said numbers and the terminal velocity can be studied in depth.
- The rising of multiple droplets in close proximity could be simulated to see whether a higher dispersed-phase concentration affects the rate at which creaming occurs.

Bibliography

[1] Krog N. Emulsifiers and emulsions in dairy foods. In *Encyclopedia of Dairy Sciences*, pages 891–900. Elsevier, Oxford, 2002.

[2] Raya S.A., Ismail M.S., Abdelazim A.A., and Abubakar A.U. A critical review of development and demulsification mechanisms of crude oil emulsion in the petroleum industry. *Journal of Petroleum Exploration and Production Technology*, 2020.

[3] Depree J.A. and Savage G.P. Physical and flavour stability of mayonnaise. *Trends in Food Science I& Technology*, 12(5), 2001.

[4] Khan M.Y., Abdul Karim Z. A., and Hagos F.Y. Current trends in water-in-diesel emulsion as a fuel. *TheScientificWorldJournal*, 2014:527472, 01 2014.

[5] Bera B., Khazal R., and Schroën K. Coalescence dynamics in oil-in-water emulsions at elevated temperatures. *Scientific Reports*, 2021.

[6] Wasan D.T., Shah S.M., Aderangi N., Chan M.S., and McNamara J.J. Observations on the Coalescence Behavior of Oil Droplets and Emulsion Stability in Enhanced Oil Recovery. *Society of Petroleum Engineers Journal*, 18(06):409–417, 12 1978.

[7] Robins M.M. Emulsions — creaming phenomena. *Current Opinion in Colloid & Interface Science*, 5(5):265–272, 2000.

[8] Howe A.M., Mackie A.R., and Robins M.M. Technique to measure emulsion creaming by velocity of ultrasound. *Journal of Dispersion Science and Technology*, 7(2):231–243, 1986.

[9] Leal-Calderon F., Schmitt V., and Bibette J. *Emulsion Science Basic Principles*. Springer, 2nd edition, 2007.

[10] Israelachvili J. N. *Intermolecular and surface forces*. Academic Press, 2011.

[11] Fredrick E., Walstra P., and Dewettinck K. Factors governing partial coalescence in oil-in-water emulsions. *Advances in Colloid and Interface Science*, 153(1):30–42, 2010.

[12] Marrucci G. A theory of coalescence. *Chemical Engineering Science*, 24(6):975–985, 1969.

[13] Ramsey M.S. Chapter six - rheology, viscosity, and fluid types. In M.S. Ramsey, editor, *Practical Wellbore Hydraulics and Hole Cleaning*, Gulf Drilling Guides, pages 217–237. Gulf Professional Publishing, 2019.

[14] Houghton E.L., Carpenter P.W., Collicott S.H., and Valentine D.T. Chapter 1 - basic concepts and definitions. In *Aerodynamics for Engineering Students (Seventh Edition)*, pages 1–86. Butterworth-Heinemann, seventh edition edition, 2017.

[15] Silverstein T.P. The real reason why oil and water don't mix. *Journal of Chemical Education*, 75, 1998.

[16] Rehm B., Drilling Consultant, Haghshenas A., Paknejad A.S., and Schubert J. Chapter two - situational problems in mpd. In *Managed Pressure Drilling*, pages 39–80. Gulf Publishing Company, 2008.

[17] Dusenbery D.B. *Living at Micro Scale*. Harvard University Press, 2011.

[18] Krüger T., Kusumaatmaja H., Kuzmin A., Shardt O., Silva G., and Viggen E. M. *The Lattice Boltzmann Method: Principles and Practice*. Springer Publishing, 2018.

[19] Anwar S. Lattice boltzmann modeling of buoyant rise of single and multiple bubbles. *Computers & Fluids*, 88:430–439, 2013.

[20] Shan X. and Chen H. Lattice boltzmann model for simulating flows with multiple phases and components. *Physical review E*, 47(3):1815, 1993.

[21] Shan X. and Doolen G. Multicomponent lattice-boltzmann model with interparticle interaction. *Journal of Statistical Physics*, 1995.

[22] Gong S. and Cheng P. Numerical investigation of droplet motion and coalescence by an improved lattice boltzmann model for phase transitions and multiphase flows. *Computers & Fluids*, 53:93–104, 2012.

[23] Bhaga D. and Weber M.E. Bubbles in viscous liquids: shapes, wakes and velocities. *Journal of Fluid Mechanics*, 105:61–85, 1981.

[24] Suga K., Kuwata Y., Takashima K., and Chikasue R. A d3q27 multiple-relaxation-time lattice boltzmann method for turbulent flows. *Computers & Mathematics with Applications*, 69(6):518–529, 2015.

[25] Nekoeian S., Goharrizi A.S., Jamialahmadi M., Jafari S., and Sotoudeh F. A novel shan and chen type lattice boltzmann two phase method to study the capillary pressure curves of an oil water pair in a porous media. *Petroleum*, 4(3):347–357, 2018.

[26] Chen L., Kang Q., Mu Y., He Y., and Tao W. A critical review of the pseudopotential multiphase lattice boltzmann model: Methods and applications. *International Journal of Heat and Mass Transfer*, 76:210–236, 2014.

[27] Zhen-Hua C. and Tian-Shou Z. A pseudopotential-based multiple-relaxation-time lattice boltzmann model for multicomponent/multiphase flows. *Acta Mechanica Sinica*, 28, 2012.